EXPERIMENTAL STUDY ON AIR SOURCE HEAT PUMP COUPLED CAPILLARY FLOOR RADIANT HEATING

Jianhui Niu[1], Chenyang Zhang[1], Yuzhou Wu[1], Zelong An[1], Shuxue Xu[*2],

[1] Department of Energy Engineering, Hebei University of Architecture, Zhangjiakou 075000, China

[2] College of Environmental and Energy Engineering, Beijing University of Technology, Beijing 100124, China

[*] Shuxue Xu; E-mail: xsx@bjut.edu.cn

In the process of global energy sustainable development, increasing the utilization of renewable energy in buildings and constructing zero-carbon buildings has become one of the important ways to alleviate global warming. In this situation, air source heat pumps are widely used because of its energy saving and stable performance. Air source heat pump coupled capillary floor radiant heating ***(ACFRH)*** *uses refrigerant as a heat transfer medium to directly heat the room floor, with no pump consumption and secondary heat transfer loss. In order to better study its temperature and heating characteristics under different capillary spacing and different outdoor temperature, an* ***ACFRH*** *experimental device was built in the artificial environment control room. The results show that the smaller the capillary spacing, the greater the vertical temperature difference of the floor. When the outdoor ambient temperature is -5 ℃ and the capillary spacing is 80 mm, the vertical temperature difference is 2.3 ℃, the surface temperature difference at different horizontal positions is 0.8 ℃, and 6.4 ℃ from the compressor discharge section to the condensate outlet section. The heating capacity and heating COP of the system are maintained at about 1.99kW and 3.85, respectively.*

Keywords: *air source heat pump; capillary floor radiant; temperature characteristic; heating performance*

1. Introduction

Due to the increase of energy consumption, the problem of global warming has become increasingly prominent. The total energy consumption of the construction industry accounts for about 40 % of the total global carbon emissions and 36 % of the total global energy consumption [1]. Heating energy consumption accounts for 50 % of the world's total energy consumption, and 46 % of building energy consumption is mainly used for space and water heating [2]. At present, China is the world's largest energy consumer [3]. The total energy consumption of China's building operation accounts for about 25 % of the country's total energy consumption, a large part of which is used for heating and cooling [4-5]. Building heating can use various forms of renewable energy, including solar energy, heat pump, biomass energy and wind energy, making it closer to green zero-carbon buildings [6]. With the goal of "2030 Carbon Peak" and "2060 Carbon Neutrality" being proposed in China, the

air source heat pumps (ASHPs) are widely used in northern China and has become an important technical equipment for winter heating [7-8]. Due to its energy saving, environmental protection, stable performance, and convenient use [9], it is expected that by 2035, ASHPs will account for 24 % of the heating demand in the northern region of China [10]. In order to better meet people's growing demand for thermal comfort, different types of ASHP heating terminals have emerged in recent years [11-16]. Currently, the traditional heating terminals used in ASHPs mainly include warm air heating, radiator heating, and hot water floor radiant heating. However, the indoor air temperature at the terminal of the fan coil unit has a large vertical gradient and a strong blowing sensation, resulting in poor indoor thermal comfort [17-18]. Experimental results show that at the same operating temperature, the energy efficiency of a refrigerant direct radiation heating system is 34.75% higher than that of a convective heat transfer system [19]. For the radiator heating, the indoor temperature distribution is not uniform, and the temperature gradient near the radiator is significantly higher than that in other places [20-21]. The hot water circulation heating system has high power consumption, complex system, and the risk of freezing and cracking in winter.The using conditions of the hot water terminal of the ASHP are limited.

In recent years, more and more attentions have been paid for direct condensing ASHP heating system for its advantages such as no secondary medium heat transfer loss, no additional pump power consumption, and no risk of freezing and cracking in winter. Shao et al. [22] examined the thermal stability, energy & exergy efficiencies and the economic performance of the ASHP system with a direct condensation radiation heating panel, the *COP* is 2.4 in the typical heating condition. Dong et al. [23] proposed and investigated the solar integrated air source heat pump (SIASHP) with R407c for radiation floor heating without water (RFHW). The average *COP* of SIASHP is 2.94 ranging from 2.15 to 3.99. A new direct expansion ASHP heating system with gravity driven radiator as heating terminal was developed by Wang et al. [24], of which PMV is maintained in the range of -0.5 ~ 0.5, and the PPD is less than 10 %. Zhao et al. [25] set up the radiation terminal experimental platform and studied that the power consumption of the capillary network radiation heating system is 45 % lower than that of the common hot water floor radiation heating system. The capillary floor radiant heating system uses high temperature refrigerant as heat transfer medium directly introduced into the floor to heat room. Zeng et al.[26] was the first to study direct floor radiant heating ASHP system in China. Cui et al. [27] carried out the experimental research for an ASHP with direct floor radiant heating system, the results showed that when heating indoors, the heating speed is fast, and the indoor temperature is uniform. Zheng et al. [28] proposed a refrigerant direct condensation floor radiation heating system with ASHP using phase change materials, which shows that when the surface temperature is higher than 26.0 ℃, the thermal comfort is better. Niu et al. [29] proposed a capillary direct floor radiant ASHP system, experimental research has been conducted to its low-temperature heating process and normal heating process when the capillary spacing is 100 mm. However, the influence of different capillary spacing on floor temperature and system performance has not been thoroughly studied. In this paper, an ASHP coupled capillary floor radiant heating (ACFRH) system was proposed and the experimental device was built in laboratory.The temperature variation characteristics of the capillary floor and the heating performance of the unit under different outdoor temperature and capillary spacing were studied in order to further broaden the application of ASHP as an energy-saving product.

2. Experimental device construction

The experimental device was built in the artificial environment control room, which includes an indoor environment control room and an outdoor environment control room. Both the indoor and outdoor temperature can be controlled at -15 ℃ ~ 40 ℃ with an accuracy of ± 0.1 ℃; The humidity can be controlled at 30 % ~ 85 % with an uncertainty of 5%.

The ACFRH system consists of an ASHP outdoor unit and a capillary floor radiant heating terminal (**CFRT**). The outdoor unit was composed of a rolling rotor compressor with a rated power of 1.0 HP, a finned tube heat-exchanger, an electronic expansion valve (EEV) and a four-way valve. The capillary floor was built mainly with parallel copper capillary. Using R410A as refrigerant, and the outlet super-heat of the evaporator was control at 5~8 ℃ through EEV. The experimental device is shown in Fig.1.

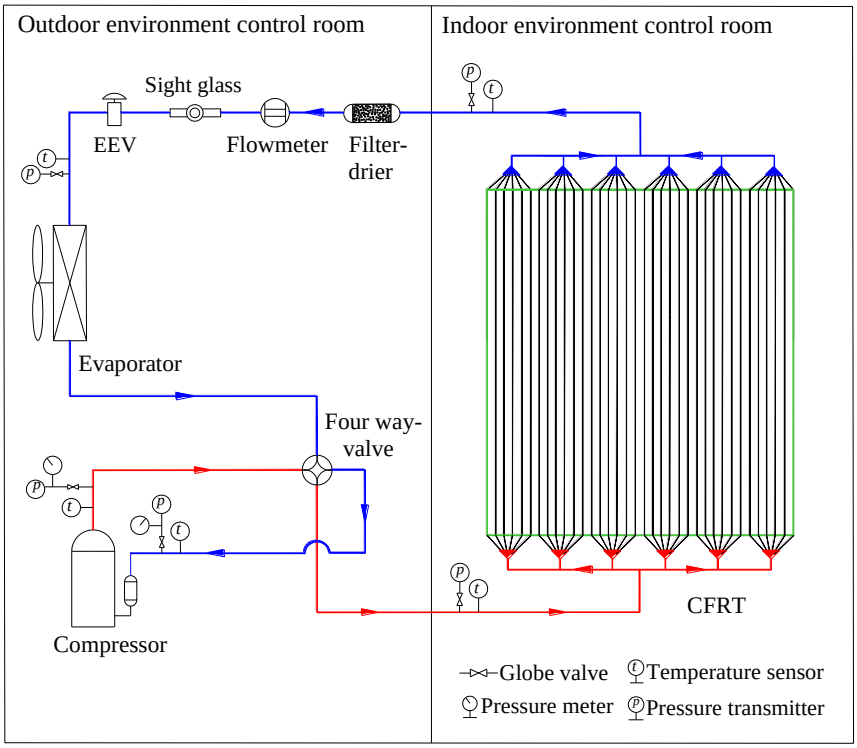

Fig. 1. Experimental device of capillary floor radiation heating system with ASHP

In the indoor environment control room, a capillary floor radiant heating floor with a size of 2 m (L)×1.5 m (W) was built. From the floor of the indoor environment control room, the following are laid in sequence: 50 mm polystyrene insulation board, 0.04 mm aluminum foil mirror reflective film, wire mesh, capillary copper tubes with an outer diameter of 4 mm and a thickness of 0.3 mm and cement mortar layer with a thickness of 20 mm. In order to ensure the uniformity of liquid separation, 6 groups of 6 branches of liquid separators were used, with a total of 36 parallelly arranged capillaries. In order to adjust the capillary spacing, a globe valve was installed at the inlet of each capillary. An artificial chamber of 2 m (L) × 1.5 m (W) × 1.8 m (H) was built above the capillary radiant heating floor. It was composed of polystyrene insulation boards. Fig.2. is the photo of the experimental device.

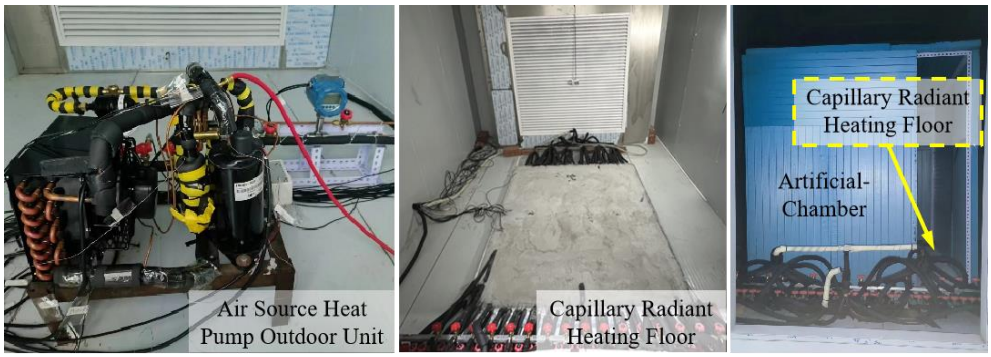

Fig. 2. Photos of the experimental device

3. Measuring points arrangement and instrument

The floor temperature is stabilized at about 20 ℃ before the heat pump is turned on. When the outdoor temperature is 5 ℃, 0 ℃, -5 ℃ and the capillary spacing is 40 mm, 80 mm and 120 mm respectively, the temperature characteristic of the capillary floor and the heating performance of the heat pump unit were studied.

Fig.3. is the floor temperature measurement points arrangement. There are 36 capillaries arranged in parallel, numbered #1 ~ #36 from left to right. When the capillary spacing is 40 mm, the globe valves are all opened; When the capillary spacing is 80 mm, the globe valves of 18 capillaries in #1, #3, #5, #7,... #35 are opened; When the capillary spacing is 120 mm, the globe valves of #1, #4, #7, #10, #13, #16, #19, #21, #25, #27, #31, #34 are opened, a total of 12 capillaries. Regardless of capillary spacing, the temperature measuring points of the capillary floor is fixed and not affected by the valve switching. It is divided into three layers from top to bottom, each layer has five same measuring points. The measuring points of the first layer are located on the surface of the cement floor, and the measuring points are numbered 1, 2, 3, 4 and 5, respectively. The second layer is located in the 10 mm thick cement mortar layer, and the measuring points are 1′, 2′, 3′, 4′ and 5′, respectively. The third layer is located on the outer wall of the capillary, and the measuring points are 1″, 2″, 3″, 4″ and 5″, respectively.

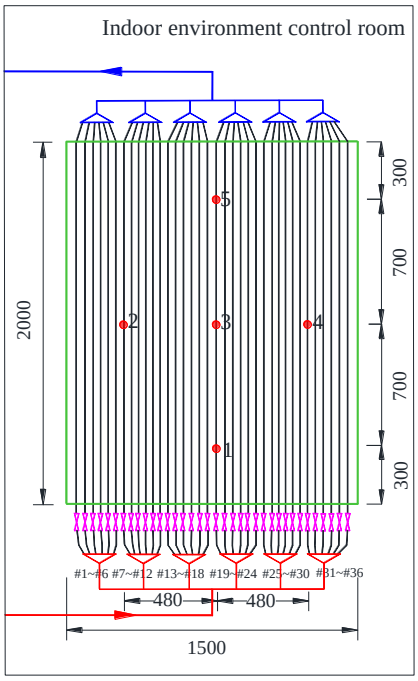

Fig. 3. The arrangement of temperature measuring points of the capillary floor

Temperature and pressure sensors are arranged at the inlet and outlet of the main equipment of the unit. The parameters such as compressor suction & discharge temperature and pressure, condenser inlet & outlet temperature and pressure, compressor power, and refrigerant mass flow rate are monitored. The data are collected and recorded by Agilent 34972A. The performance parameters of each measuring instrument are shown in Tab.1.

Tab. 1. Instrumentation performance parameters

Parameters	Model	Full scale	Accuracy
Pressure	520.933S033401W	-0.1 ~ 4.0 MPa	± 0.2%
Temperature	T-Thermocouple	-150 ~ 200 ℃	±0.2 ℃
	PT100	-150 ~ 150 ℃	±0.15 ℃
Compressor power	PD6000-Y30	0 ~ 10 kW	0.5%
Flow meter	LW-4Z1M2SDSR	0.04 ~ 0.25 m^3/h	± 1%
Data acquisition	Agilent34972A		± 0.2%

4. Data analysis and error handling

During the experiment, the direct measurement of physical quantities includes temperature, pressure, compressor power, refrigerant flow. And the required indirect refrigerant enthalpy can be obtained by the physical parameter software REFPROP 9.1. The heating capacity of the system is obtained by multiplying the enthalpy difference of the refrigerant at the inlet and outlet of the condenser by the mass flow rate of the refrigerant.

$$Q = q(h_i - h_o) \tag{1}$$

Where, Q is the heating capacity of the system, kW; q is the mass flow rate of refrigerant, kg/s; h_i and h_o are the enthalpy of the refrigerant at the inlet and outlet of the condenser respectively, kJ/kg.

The heating *COP* (coefficient of performance):

$$COP = \frac{Q}{P} \tag{2}$$

Where, P is compressor power, kW.

If Y (output) cannot be measured directly, the estimated value y has a functional relationship with other measured values x_1, x_2,..., x_n (input) :

$$y = f(x_1, x_2, \cdots, x_n) \tag{3}$$

The uncertainty u_y of the estimated value y is the combination of all uncertainty components (corresponding input x_1, x_2 ,..., x_n), which is expressed by the combined standard uncertainty $u_c(y)$. If the uncertainty of all input quantities are independent of each other, the combined standard uncertainty calculation formula is calculated according to formula (4):

$$u_c(y) = \sqrt{\sum_{i=1}^{N} \left(\frac{\partial f}{\partial x_i} \right)^2 u_{xi}^2} \tag{4}$$

Where, u_{xi} is the standard uncertainty; $\frac{\partial f}{\partial x_i}$ is the error transfer coefficient.

Therefore, it can be known:

$$Q = q(h_{\mathrm{i}} - h_{\mathrm{o}}) = f(q, p_{\mathrm{i}}, t_{\mathrm{i}}, p_{\mathrm{o}}, t_{\mathrm{o}}) \tag{5}$$

$$COP = \frac{Q}{P} = \frac{q(h_{\mathrm{i}} - h_{\mathrm{o}})}{P} = f(q, p_{\mathrm{i}}, t_{\mathrm{i}}, p_{\mathrm{o}}, t_{\mathrm{o}}, P) \tag{6}$$

The error between heating capacity Q and heating COP of the system can be calculated:

$$u_Q = \sqrt{\left(\frac{\partial f}{\partial q}u_q\right)^2 + \left(\frac{\partial f}{\partial t_{\mathrm{i}}}u_{t_{\mathrm{i}}}\right)^2 + \left(\frac{\partial f}{\partial t_{\mathrm{o}}}u_{t_{\mathrm{o}}}\right)^2 + \left(\frac{\partial f}{\partial p_{\mathrm{i}}}u_{p_{\mathrm{i}}}\right)^2 + \left(\frac{\partial f}{\partial p_{\mathrm{o}}}u_{p_{\mathrm{o}}}\right)^2} \tag{7}$$

$$u_{COP} = \sqrt{\left(\frac{\partial f}{\partial q}u_q\right)^2 + \left(\frac{\partial f}{\partial t_{\mathrm{i}}}u_{t_{\mathrm{i}}}\right)^2 + \left(\frac{\partial f}{\partial t_{\mathrm{o}}}u_{t_{\mathrm{o}}}\right)^2 + \left(\frac{\partial f}{\partial p_{\mathrm{i}}}u_{p_{\mathrm{i}}}\right)^2 + \left(\frac{\partial f}{\partial p_{\mathrm{o}}}u_{p_{\mathrm{o}}}\right)^2 + \left(\frac{\partial f}{\partial P}u_P\right)^2} \tag{8}$$

$$u_{rel,Q} = \frac{u_Q}{Q} \tag{9}$$

$$u_{rel,COP} = \frac{u_{COP}}{COP} \tag{10}$$

Where, u_q, $u_{t\mathrm{i}}$, $u_{t\mathrm{o}}$, $u_{p\mathrm{i}}$, $u_{p\mathrm{o}}$, u_P are the parameter uncertainty; u_Q and u_{COP} are combined standard uncertainty (also known as comprehensive uncertainty); $u_{rel,\ Q}$ and $u_{rel,\ COP}$ are the related expanded uncertainty (measurement error). After calculation, the measurement error of heating capacity Q and heating COP are 2.9 % and 4.1 %, respectively. The errors of heating capacity Q and heating COP are related to the directly measured parameters such as refrigerant flow, the pressure & temperature and the power of the compressor. The impact of measurement errors has been eliminated in the data of results and analysis.

5. Experimental results and analysis

Fig.4. shows the temperature variation of the floor surface when the capillary spacing l is 80 mm and the outdoor environment temperature t_{o} is 5 ℃, 0 ℃ and -5 ℃, respectively. It can be seen from Fig.4 that after the start-up of the heat pump system, the floor surface temperature rises significantly. and the temperature rise rates of 2,3 and 4 are basically the same; When the outdoor temperature is 5 ℃, the temperature rise rates of 1, 2~4, and 5 are 1.6 ℃ / 10min, 1.2 ℃ / 10min, and 0.5 ℃ / 10min, respectively; When the outdoor temperature is 0 ℃, the temperature rise rates of the three is 1.2 ℃ / 10min, 0.5 ℃ / 10min , 0.3 ℃ / 10min，respectively. When the outdoor temperature is -5 ℃, the temperature rise rates is 0.9 ℃ / 10min, 0.3 ℃ / 10 min, and 0.2 ℃ / 10min, respectively. The temperature rise of measuring point 1 is the fastest, 5 is the slowest, and 2 ~ 4 is between them. This is because measuring point 1 is located in the compressor vapour discharge section, 5 is located in the condensate outlet section, and 2-4 are located in the middle saturated section.

With the decrease of outdoor temperature, the final stable temperature of the floor surface

decreases. However, under different outdoor ambient temperature, the temperature of measuring point 1 is always the highest, the temperature of measuring point 5 is always the lowest, and the temperature of measuring points 2, 3, 4 are close. When the outdoor temperature is 5 ℃, the temperature of measuring point 1 is maintained at 33.8 ℃. 2, 3 and 4 are maintained at 30.1 ℃, 29.7 ℃ and 29.3 ℃, respectively. The temperature difference of the three points does not exceed 0.8 ℃ with good temperature uniformity. The temperature of measuring point 5 is maintained at 24.8 ℃. The average surface temperature rise rate is 1.2 ℃ / 10 min. When t_o=0 ℃, the temperature of measuring point 1 is maintained at 29.6 ℃. Compared with that of t_o=5 ℃, the temperature is reduced by 4.2 ℃. The temperature of measuring points 2, 3 and 4 is maintained at 24.2 ℃, 24.6 ℃ and 24.8 ℃, respectively, and the temperature difference does not exceed 0.6 ℃. Compared with that of t_o=5 ℃, the temperature is reduced by about 5.0 ℃. The temperature of measuring point 5 is maintained at 22.8 ℃ with a decrease of 2.0 ℃. The average surface temperature rise rate is 0.7 ℃ / 10 min. When t_o=-5 ℃, the temperature of measuring point 1 is maintained at 27.9 ℃. The temperature of measuring points 2, 3 and 4 are close, they are maintained at 22.9 ℃, 22.8 ℃ and 23.6 ℃, respectively, and the temperature difference does not exceed 0.8 ℃. The temperature of measuring point 5 is maintained at 21.5 ℃. Compared with measuring point 1, the temperature difference between the two is 6.4 ℃. The average surface temperature rise rate is 0.5 ℃ / 10 min.The temperature variation of measuring points 1, 3, 5 and measuring points 2, 3, 4 reflects the surface temperature distribution characteristics of the capillary radiant floor heating terminal in the orthogonal two directions to a certain extent.

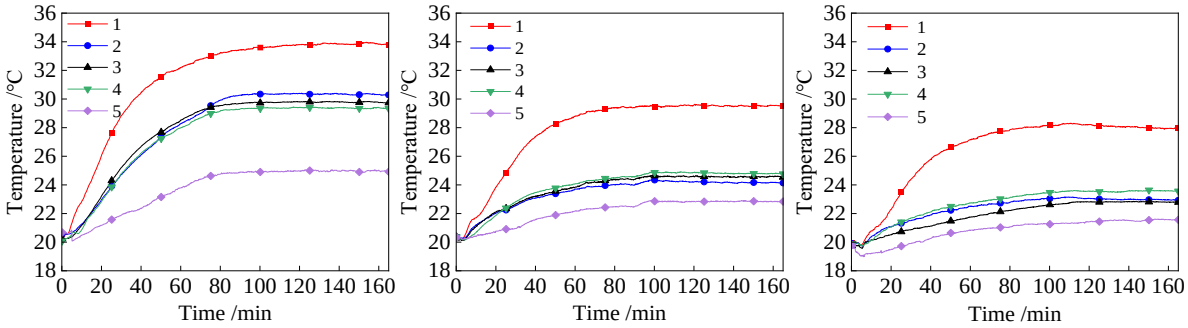

(a) t_o= 5 ℃ (b) t_o= 0 ℃ (c) t_o= -5 ℃

Fig. 4. The variation of cement surface temperature under different outdoor temperature when *l*= 80mm

Fig.5. shows the temperature variation of different vertical thicknesses of the floor at different capillary spacing when t_o= -5 ℃. The measuring points 3 , 3 ′ and 3 ″ are located on the surface of the cement floor, 10 mm thick cement mortar layer, and the outer wall of the capillary, respectively. From Fig.5 that when *l*=40 mm, the temperature of the measuring points 3, 3 ′ and 3″ are maintained at 24.4 ℃, 25.3 ℃ and 27.5 ℃, respectively, and the average temperature rise rates are 0.36 ℃ / 10 min, 0.44 ℃ / 10 min and 0.65 ℃ / 10 min, respectively. When *l*=80 mm, they are maintained at 22.8 ℃, 23.8 ℃ and 25.1 ℃, respectively, and the average temperature rise rates are 0.29 ℃ / 10 min, 0.41 ℃ / 10 min and 0.55 ℃ / 10 min, respectively. When *l*=120 mm, they are maintained at 21.4 ℃, 22.5 ℃ and 23.3 ℃, respectively, and the average temperature rise rates are 0.09 ℃ / 10 min, 0.15 ℃ / 10 min and 0.20 ℃ / 10 min, respectively. The maximum temperature difference between measuring points 3″ and 3 under the spacing of 40 mm, 80 mm and 120 mm are 3.4 ℃, 2.5 ℃ and 1.9 ℃, respectively, that is, the smaller the capillary spacing, the more obvious the vertical temperature stratification. From above analysis, we can see that the smaller the capillary spacing, the higher the vertical temperature and the greater the vertical temperature difference. Due to the thermal inertia of the cement floor, the vertical heat transfer process from the outer wall of the capillary to the floor surface would naturally

have a certain delay and lag, which also causes the difference between the vertical temperature difference and the temperature rise rate of each layer.

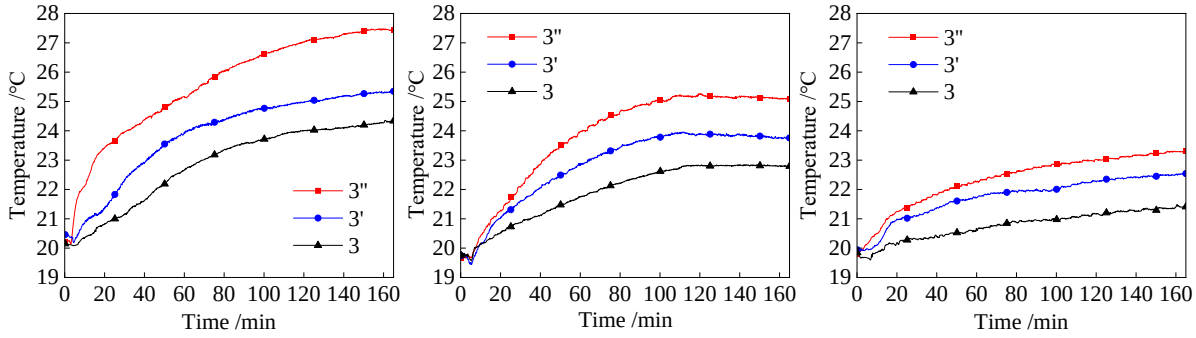

(a) l = 40 mm (b) l = 80 mm (c) l = 120 mm

Fig. 5. Vertical temperature variation of floor under different capillary spacing when t_o=-5 ℃

Fig.6. ~ Fig.8. are the temperature variation of measuring points 1, 3 and 5 under different capillary spacing and outdoor temperature. From Fig.6. ~ Fig.8, we can see that the smaller the capillary spacing is, the faster the temperature rise rate of each measuring point is and the higher the temperature is. The higher the ambient temperature, the higher the temperature of different measuring points. When t_o=-5 ℃ and l= 40 mm, the temperature of measuring point 1 can reach 30.4 ℃, and the temperature rise rate is 1.38 ℃ / 10 min. Compared with the 80 mm spacing, the two are 2.2 ℃ and 0.28 ℃ / 10 min higher, respectively; Compared with the 120 mm spacing, they are 4.3 ℃ and 0.72 ℃ / 10 min higher, respectively, and the temperature rise is obvious. When l= 40 mm and t_o= 5 ℃, it is stable at 35.7 ℃, about 3.3 ℃ higher than that of when t_o= 0 ℃, and 5.2 ℃ higher than that of when t_o= -5 ℃. The measuring point 3 can reach 24.4 ℃, and the temperature rise rate is 0.36 ℃ / 10 min. The two are 1.6 ℃ and 0.07 ℃ / 10 min higher than that of l=80 mm, and 3.0 ℃ and 0.27 ℃ / 10 min higher than that of l=120 mm, respectively. When l= 40 mm and t_o= 5 ℃, it is maintained at about 31.6 ℃, about 3.4 ℃ higher than that of when t_o= 0 ℃, and 7.3 ℃ higher than that of when t_o= -5 ℃. The measuring point 5 can reach 22.5 ℃, and the temperature rise rate is 0.22 ℃ / 10 min. The two are 0.92 ℃ and 0.06 ℃ / 10 min higher than the 80 mm spacing, and 1.38 ℃ and 0.13 ℃ / 10 min higher than the 120 mm spacing, respectively. When l= 40 mm and t_o= 5 ℃, it is maintained at about 27.1 ℃, about 2.6 ℃ higher than that of when t_o= 0 ℃, and 4.6 ℃ higher than that of when t_o= -5 ℃.

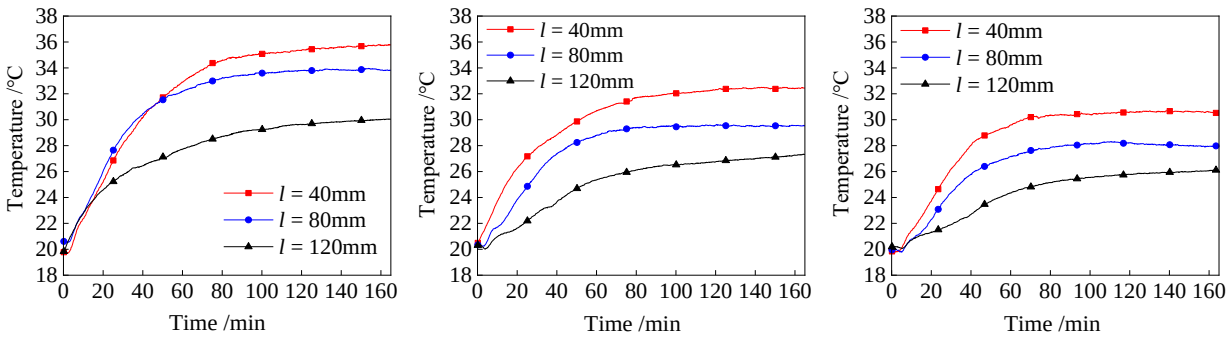

(a) t_o= 5 ℃ (b) t_o= 0 ℃ (c) t_o= -5 ℃

Fig. 6. The temperature variation of measuring point 1 at different capillary spacing and outdoor temperature

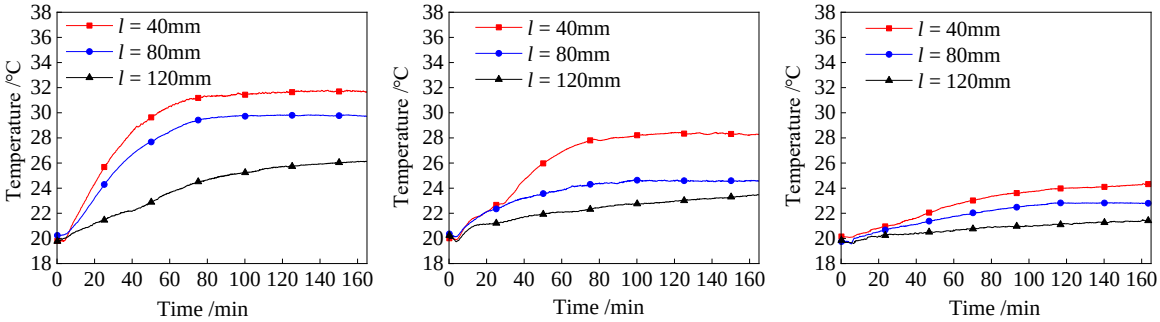

(a) t_o= 5 ℃ (b) t_o= 0 ℃ (c) t_o= -5 ℃

Fig. 7. The temperature variation of measuring point 3 at different capillary spacing and outdoor temperature

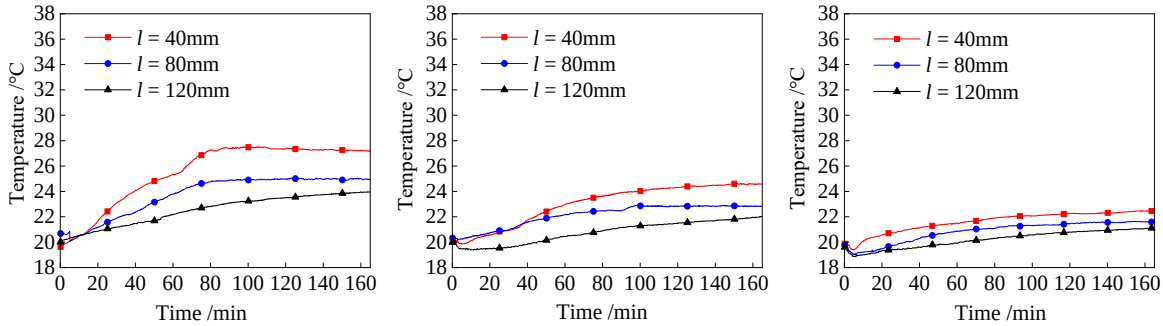

(a) t_o= 5 ℃ (b) t_o= 0 ℃ (c) t_o= -5 ℃

Fig. 8. The temperature variation of measuring point 5 at different capillary spacing and outdoor temperature

Fig.9.(a) shows the variation of the heating capacity of the ACFRH system under different capillary spacing and outdoor temperature. It can be seen from Fig.9.(a) that the smaller the capillary spacing is, the greater the heating capacity is, and the lower the outdoor ambient temperature is, the smaller the heating capacity is. When t_o= 5 ℃ and l=40 mm, the heating capacity of the system is maintained at 2.78 kW, about 0.26 kW higher than that of when l=80 mm and about 0.54 kW higher than that of when l=120 mm. When the outdoor temperature is 0 ℃, the heating capacity is maintained at 2.56 kW at 40 mm spacing, 2.31 kW at 80 mm spacing, and 2.03 kW at 120 mm spacing. When the outdoor temperature is -5 ℃, the heating capacity is maintained at 2.23 kW at 40 mm spacing, 1.99 kW at 80 mm spacing, and 1.71 kW at 120 mm spacing. When the outdoor temperature is -5 ℃, the heating capacity at 80 mm spacing is 12.1 % lower than that at 40 mm spacing, and the heating capacity at 120 mm spacing is 16.3 % lower than that at 80 mm spacing. When the capillary spacing is 80 mm, the heating capacity at the outdoor temperature of -5 ℃ is 16.2 % lower than that at the outdoor temperature of 0 ℃, and the heating capacity at the outdoor temperature of 0 ℃ is 9.1 % lower than that at the outdoor temperature of 5 ℃.

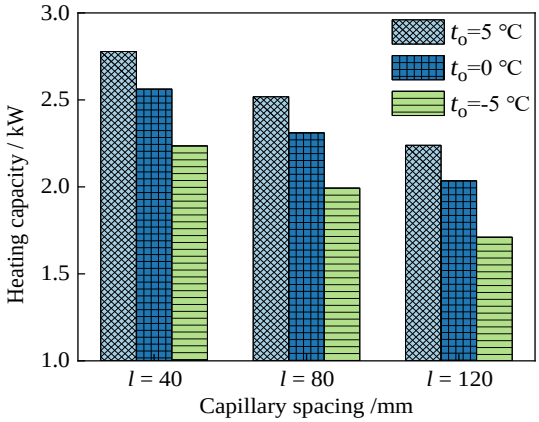

(a) Heating capacity

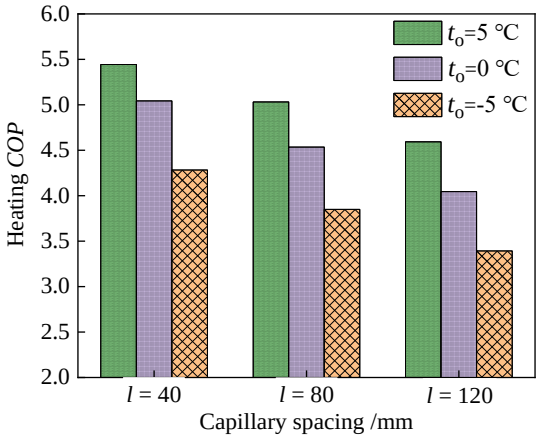

(b) Heating *COP*

Fig. 9. The variation of heating capacity and *COP* under different capillary spacing and outdoor temperature

Fig.9.(b) shows the heating *COP* variation under different capillary spacing and outdoor temperature. Comparing with Fig.9.(a), it can be seen that the variation regularity of the heating *COP* of the system is basically the same as that of the heating capacity. The lower the outdoor environment temperature is and the larger the capillary spacing is, the lower the heating *COP* is. When t_o= 5 ℃, the heating *COP* is stable at 5.44, 5.03, and 4.59 when *l*=40 mm, 80 mm, and 120 mm,respectively. When t_o= -5 ℃, the heating *COP* is stable at 4.28, 3.85, and 3.39 when *l*=40 mm, 80 mm, and 120 mm, respectively. When t_o= -5 ℃, the heating *COP* at 80 mm spacing is 11.2 % lower than that of at 40 mm spacing, and the heating *COP* at 120 mm spacing is 13.6 % lower than that of at 80 mm spacing. When *l*=80 mm, the heating *COP* at the outdoor temperature of -5 ℃ is 17.7 % lower than that of at the outdoor temperature of 0 ℃, and the heating *COP* at the outdoor temperature of 0 ℃ is 11.0 % lower than that of at the outdoor temperature of 5 ℃.

The air source water-loop heat pump generally for ambient temperature is below -12 ℃, the heating *COP* will be smaller than 2.0 . Furthermore, the discharge temperature is too high (higher than 120 ℃) and the refrigerant flow mass decrease significantly, these heat pump systems have difficulty running efficiently, reliably and stably [30]. The system *COP* fluctuates between 1.7 and 3.5 when the ambient temperature varies from -9.2 ℃ to 14 ℃, and the mean value of the *COP* is about 2.59 for the ASHP with refrigerant-heated panel [31]. Fans were introduced to direct-condensation heating panel to enhance the forced convection, and the system *COP* increased from 2.86 to 3.11 with the increased indoor air flowrate [32]. However, it increases the fan power consumption and noise . When the outdoor temperature is -5 ℃, the *COP* can reach 3.55 for the ASHP with refrigerant directly condensation wire mesh type terminal [33]. However, the wire mesh needs to be hung up, occupying room space, and more easily be touched to deformed.

6. Conclusions

The air source heat pump coupled with capillary floor radiant heating with refrigerant as the heat exchange medium to heat the room floor. The experiment was carried out under different outdoor ambient temperature and different capillary spacing, and the conclusions are as follows:

1) With the decrease in outdoor temperature, the surface temperature rise rate decreases. When the outdoor temperature is -5 ℃ and the capillary spacing is 80 mm, the average floor surface temperature rise rate is 0.5 ℃ / 10 min, and the floor surface temperature can reach 27.9 ℃, which is 1.7 ℃ lower than that of when the outdoor temperature is 0 ℃. The temperature difference between

different measuring points at the same horizontal position does not exceed 0.8 ℃. From the compressor discharge section to the condensate outlet section, the maximum temperature difference is 6.4 ℃ of 80mm capillary tube spacing under the outdoor temperature of -5 ℃.

2) The smaller the capillary spacing, the higher the vertical temperature and the greater the vertical temperature difference. Due to the thermal inertia of the cement floor, the vertical heat transfer process from the outer wall of the capillary to the floor surface would naturally have a certain delay and lag. When the outdoor temperature is -5 ℃ and the capillary spacing is 80 mm, the maximum temperature difference between the capillary wall and the floor surface is 2.3 ℃. They are maintained at 22.8 ℃, 23.8 ℃ and 25.1 ℃, respectively, and the average temperature rise rates are 0.29 ℃ / 10 min, 0.41 ℃ / 10 min and 0.55 ℃ / 10 min, respectively.

3) The heating capacity and heating *COP* of the heat pump system decrease with the decrease of outdoor temperature, and increase of capillary spacing. When the outdoor temperature is -5 ℃ and the capillary spacing is 80 mm, the heating capacity can be maintained at about 1.99 kW, and the heating *COP* can be stabilized at about 3.85.

Acknowledgments

This project was funded by the Doctoral Research Initiation Fund Project of Hebei University of Architecture (Grant No. B-202303), the Postgraduate Innovation Fund Project of Hebei University of Architecture (Grant No. XY2024090).

Declaration of Interest Statement

The authors declare that they have no known competing financial interests or personal relationships that could have appeared to influence the work reported in this paper.

Nomenclature

h_i	refrigerant inlet enthalpy (kJ/kg)
h_o	refrigerant outlet enthalpy (kJ/kg)
l	spacing between copper capillary tubes (mm)
P	compressor power (kW)
Q	heating capacity (kW)
q	refrigerant volume flow (m^3/h)
t	temperature (℃)
u_{xi}	precision of parameter uncertainty
$u_{rel,\ Q}$	precision of Q error
$u_{rel,\ COP}$	precision of *COP* error
ASHP	Air source heat pump
ACFRH	ASHP coupled capillary floor radiant heating
COP	Coefficient of performance
CFRT	Capillary floor radiant heating terminal
EER	Energy efficiency ratio
PMV	Predicted mean vote
PPD	Predicted percentage of dissatisfied
RFHW	Radiant floor heating without water
SIASHP	Solar integrated air source heat pump

References

[1] Ke, Z. K., *et al*., Energy Consumption and Carbon Emissions of Nearly Zero-Energy Buildings in Hot Summer and Cold Winter Zones of China, *Sustainability*, *15* (2023), 14, 11453

[2] Wang, N., *et al*., Performance Research and Multi-Objective Optimization of Concentrating Photovoltaic/Thermal Coupled Air Source Heat Pump Heating System, *Energy*, *296* (2024), 131008

[3] Cao, X. D., *et al*., Building Energy-Consumption Status Worldwide and the State-of-the-Art Technologies for Zero-Energy Buildings During the Past Decade, *Energy and Buildings*, *128* (2016), pp.198-213

[4] Song, Y. Y., *et al*., Using the Degree-Day Method to Analyze Central Heating Energy Consumption in Cities of Northern China, *Sustainability*, *16* (2024), 3, 1008

[5] Yu, Y. Z., *et al*., Effect of Implementing Building Energy Efficiency Labeling in China: A Case Study in Shanghai, *Energy Policy*, *133* (2019), 110898

[6] Zhang, S., *et al*., Renewable Energy Systems for Building Heating, Cooling and Electricity Production with Thermal Energy Storage, *Renewable and Sustainable Energy Reviews*, *165* (2022), 112560

[7] Zeng, Y. J., *et al*., Research on Energy Savings of an Air-Source Heat Pump Hot Water System in a College Student's Dormitory Building, *Sustainability*, *15* (2023), 13, 10006

[8] Chen, Q., *et al*., Energy, Emissions, Economic Analysis of Air-Source Heat Pump with Radiant Heating System in Hot-Summer and Cold-Winter Zone in China, *Energy for Sustainable Development*, *70* (2022), pp.10-22

[9] Wu, C.L., *et al*., Low-Temperature Air Source Heat Pump System for Heating in Severely Cold Area: Long-Term Applicability Evaluation, *Building and Environment*, *208* (2022), 108594

[10] Wu, C.L., *et al*., Optimizing the Selection and Combined Operation of Multiple Air-Source Heat Pumps for Sustainable Heating Systems, *Energy and Buildings*, *310* (2024), 114052

[11] Xu, S.X., *et al*., Experimental Investigation of an Air Source Heat Pump with Multigroup Heat Pipe Radiators, *Solar Energy*, *260* (2023), pp.137-146

[12] Zheng, X.J., *et al*., Performance of the Air Source Heat Pump Assisted Solar Heating System Combined with PCM Floor, *Applied Thermal Engineering*, *239* (2024), 122115

[13] Jia, J., *et al*., Field Test on Performance of an Air Source Heat Pump System Using Novel Gravity-Driven Radiators as Indoor Heating Terminal, *Frontiers in Energy Research*, *9* (2021), 765781

[14] Bai, X.X., *et al*., An Experimental Study on Achieving Even-Frosting for an Air Source Heat Pump Using a Novel Dual-Fan Outdoor Coil, *Energy and Buildings*, *255* (2022), 111695

[15] Li, H.J., *et al*., Experimental Study on Performance of Medium-Pressure Air-Supply Heat Pump Air Conditioning System for Pure Electric Bus, *Thermal Science*, *25* Part B (2021), 3, pp.2311-2318

[16] Prashantha, B.G., *et al*., Design and Analysis of Thermoacoustic Air Source Heat Pump Water Heaters, *International Journal of Air-Conditioning and Refrigeration*, *32* (2024), 1, pp.1-14

[17] Hu, B., *et al*., Performance Evaluation of Different Heating Terminals Used in Air Source Heat Pump System, *International Journal of Refrigeration, 98* (2019), pp.274-282

[18] Ye, J.Y., *et al*., Experimental Study on the Heating and Humidifying Performance of Fan Coil Units with Humidification Modules in Severe Cold Regions, *Energy and Buildings*, *276* (2022), 112500

[19] Liu, D., *et al*., Comparative Analysis of Heating Characteristics of Convective-Radiant Systems Using Various Terminal Air Source Heat Pumps, *Energy and Buildings*, *301* (2023), 113701

[20] Hu, F.C., *et al*., Simulation and Analysis of Air Source Heat Pump Used in Different Heating Terminal of Beijing Rural House, *Procedia Engineering*, *205* (2017), pp.397-404

[21] Xu, S.X., *et al*., Investigation of Air-Source Heat Pump Using Heat Pipes as Heat Radiator, *International Journal of Refrigeration*, *90* (2018), pp.91-98

[22] Shao, S.L., *et al*., Thermodynamic and Economic Analysis of the Air Source Heat Pump System with Direct-Condensation Radiant Heating Panel, *Energy*, *225* (2021), 120195

[23] Dong, X., *et al*., Energy and Exergy Analysis of Solar Integrated Air Source Heat Pump for Radiant Floor Heating without Water, *Energy and Buildings*, *142* (2017), pp.128-138

[24] Wang, H.B., *et al*., Experimental and Numerical Study on Thermal Performance of a Novel Direct Expansion Air-Source Heat Pump Heating System, *Frontiers in Energy Research, 9* (2022), 765221

[25] Zhao, M., *et al*., Performance Comparison of Capillary Mat Radiant and Floor Radiant Heating Systems Assisted by an Air Source Heat Pump in a Residential Building, *Indoor and Built Environment, 26* (2017), 9, pp.1292-1304

[26] Zeng, Z.C., *et al*., Experimental Research and Thermodynamics Analysis of Direct Radiant Floor Heating System with Air Source Heat Pump (in Chinese), *Acta Energiae Solaris Sinica*, *32* (2011), 8, pp.1151-1157

[27] Cui, M.M., *et al*., Experimental Study on Direct Floor Radiant Heating with Air Source Heat Pump (in Chinese), *Journal of Appliance Science & Technology*, *4* (2022), pp.96-100

[28] Zheng, C.X., *et al*., Defrosting Performance Improvement of Air-Source Heat Pump Combined Refrigerant Direct-Condensation Radiant Floor Heating System with Phase Change Material, *Energies*, *13* (2020), 18, 4594

[29] Niu, J.H., *et al*., Experimental Research of Heating Characteristics on an Air Source Heat Pump System with Capillary Direct Floor Radiant, *International Journal of Refrigeration, 170* (2025), pp.224-235

[30] Xu, X.S., *et al*., ‘Coal-to-electricity’ Project is ongoing in North China, *Energy, 191* (2020), 116525

[31] Shao, S.L., *et al*., Thermal Performance Analysis of a New Refrigerant-Heated Radiator Coupled with Air-Source Heat Pump Heating System, *Applied Energy*, *247* (2019), pp.78-88

[32] Dong, J.K., *et al*., An Experimental Study on a Novel Radiant-Convective Heating System Based on Air Source Heat Pump, *Energy and Buildings, 158* (2018), 1, pp. 812-821

[33] Dang, P.F. *et al*., Performance Analysis of a New Type of Heat Pump System with Natural Convection Heat Sink (In Chinese), *Refrigeration and Air Conditioning, 36* (2022), 2, pp.196-202

Submitted: 09.11.2024.
Revised: 07.05.2025.
Accepted: 12.05.2025.